CHIN. PHYS. LETT. Vol. 34, No. 6 (2017) 068102

Efficient Visible Photoluminescence from Self-Assembled Ge QDs Embedded in Silica Matrix *

Alireza Samavati**, Zahra Samavati, A. F. Ismail**, M. H. D. Othman, M. A. Rahman, A. K. Zulhairun

Advanced Membrane Technology Research Centre, Universiti Teknologi Malaysia, Skudai 81310, Malaysia

(Received 15 February 2017)

Measuring the growth parameters of Ge quantum dots (QDs) embedded in SiO_2/Si hetero-structure is prerequisite for developing the optoelectronic devices such as photovoltaics and sensors. Their optical properties can be tuned by tailoring the growth morphology and structures, where the growth parameters' optimizations still need to be explored. We determine the effect of annealing temperature on surface morphology, structures and optical properties of Ge/SiO_2/Si hetero-structure. Samples are grown via rf magnetron sputtering and subsequent characterizations are made using imaging and spectroscopic techniques.

PACS: 81.07.Ta, 78.40.Fy, 78.55.−m DOI: 10.1088/0256-307X/34/6/068102

Tuning the density, size and visible luminescence of Ge quantum dots (QDs) is demanding for sundry applications and it is not realized without careful measuring and monitoring of the structural and optical parameters of such nanostructures. Precise control on layer thickness and annealing temperature is expected to influence the structural, morphological and emission behavior of such QDs. Lately, the emergence of advanced nanometric technology has led to the realization of QD devices.[1]

In our earlier communication, we demonstrated the role of SiO_2 matrix thickness variation on the growth of rf sputtered Ge QDs, where interfacial intermixing and strain energies are mainly attributed to the growth mechanism.[2] Furthermore, the sputtering parameter-dependent structural, morphological and optical properties of Ge/Si(100) QDs have been reported.[3] However, the accurate and comprehensive discussions on structural and optical properties of such layered nanostructure are not thoroughly scrutinized. Therefore, it is customary to inspect the post-annealing temperature-stimulated formation of Ge QDs through successive deposition of Ge/SiO_2 layers.

A self-assembled hetero-structure of Ge/SiO_2/Si layers with Ge QDs employing rf magnetron sputtering is fabricated. The samples are grown using a polycrystalline SiO_2 and Ge targets (99.999% purity) on p-type Si (100) at 200℃ substrate temperature. Before starting the deposition, the target is sputter cleaned for 10 min to remove any contaminants and to eliminate any differential sputtering effect. The hetero-structure is grown as follows: initially a layer of SiO_2 on a Si substrate, and then a thin layer of Ge on top of the SiO_2 layer is deposited. During the deposition of each layer the chamber evacuated until a pressure around 2×10^{-6} Torr. The Ge layer is grown in Ar atmosphere with 10 sccm flow rate. The total gas pressure in the chamber is kept constant at 6 mTorr during the growth process. The rf powers used for deposition of SiO_2 and the Ge layer are 100 and 200 W, respectively. The thicknesses of the SiO_2 spacer (10 nm) and Ge top-layers (5 nm) are controlled by the thin film analyzer (Filmetrics F20, USA) and deposition time. These thicknesses are calculated from the typical deposition rate of thin layers grown under similar conditions,[4,5] which are ∼9 and 6 nm/min for SiO_2 and Ge, respectively, considering a linear rate deposition.

A post-growth annealing step is applied to a subset of samples in a rapid thermal processing oven (Anneal sys, AS-One 150) in ambient nitrogen (N_2) at annealing temperature of 300 ($A_{300}S_{10}G_5$), 500 ($A_{500}S_{10}G_5$), and 700℃ ($A_{700}S_{10}G_5$) for 2 min and then cooled down spontaneously. The duration of annealing time is chosen based on our previous research, in which the higher quality samples were achieved for 2 min annealing time.[6] The maximum annealing temperature is set at 700℃ to avoid desorption of Ge. The morphological and structural properties of samples are characterized using an atomic force microscopy (SPI3800) built by Seiko Instrument Inc. (SII) and an x-ray diffraction (Bruker D8 Advance Diffractometer) using Cu-Ka_1 radiations (1.540 Å) at 40 kV and 100 mA, respectively. The scanning range of 2θ is varied from 20° to 75°. A slow speed of scanning ∼1.2°/min with a resolution of 0.011° is employed. The elemental composition of the sample is analyzed through energy dispersive in an x-ray diffractometer (EDX) attached to FESEM, JEOL, JSM-6701 F. Fourier transformed infrared (FTIR) spectra are recorded using Perkin Elmer 5DX FTIR. Raman spectroscopy using a spectrum GX (NIR, FT-Raman) system with a Nd crystal laser source having a spot size of 1 mm is performed. The room temperature PL measurement (Perkin Elmer LS 55 Luminescence Spectrometer) is carried out using a xenon flash lamp under 239 nm excitation wavelength.

The AFM images of the surface morphology and the histograms of dot diameters at annealing temper-

*Supported by the Advanced Membrane Technology Research Center of the Universities Teknologi Malaysia under Grant No R.J130000.7609.4C112, the Postdoctoral Grant, and the Frontier Materials Research Alliance.

**Corresponding author. Email: alireza.samavati@yahoo.com; afauzi@utm.my

© 2017 Chinese Physical Society and IOP Publishing Ltd

atures of 300, 500, 700℃ are shown in Fig. 1. Dots became larger at 500 and 700℃. The average dot diameter and its standard deviation are 43 nm and 1 nm at 500℃, and 54 nm and 2 nm at 700℃. The general increase in QD size upon annealing is due to the interdiffusion of oxygen and silicon between the Ge QDs and their surrounding barriers, which causes the decrease of the strain between the deposited layers followed by coalescence of clusters with close proximity and possible formation of polycrystalline dots. The dot size is the smallest at 300℃, and the average dot diameter and its standard deviation are 28 and 1 nm, respectively. The dependences of rms roughness and dot density on annealing temperature are shown as the inset of Fig. 1. Dot number densities are estimated from the average in $700 \times 700\,\mathrm{nm}^2$ area. Enhancement of number density by increasing the annealing temperature from 500 to 700℃ (0.6–$0.7 \times 10^{11}/\mathrm{cm}^2$) is attributed to the reason that increasing the annealing temperature leads to the increase of the kinetic energy of the surface atoms, which can travel a longer path and growth of more thermodynamically stable clusters in exposure to new nucleation sites.

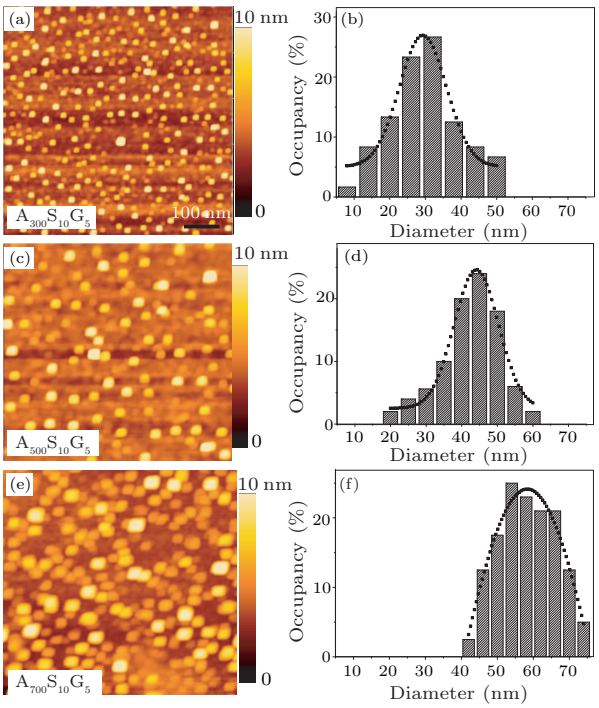

Fig. 1. AFM images and size distribution of samples at different annealing temperatures.

There is a strong correlation between dot density and surface roughness. According to the small surface roughness at 300℃, it is considered that Ge growth like the S–K mode with dot formation occurs. However, considering the reaction of SiO_2 and Si surface, we interpret the phenomenon as follows: oxygen atoms are incorporated into Ge and do not improve crystallinity at 300℃. On the other hand, the deposited SiO_2 formed Si–O bonds which promoted the Ge dots formation due to lack of adsorption site for Ge below 500℃.[7] Therefore, Ge growth like the V–W mode and higher dot density occur at 300℃.

The XRD patterns of the samples $A_{300}S_{10}G_5$, $A_{500}S_{10}G_5$ and $A_{700}S_{10}G_5$ are shown in Fig. 2(a). All the detectable peaks could be indexed as the Ge diamond structure found in the standard reference data (JCPDS 4-0545).[8] It is clearly seen that the reflection peaks become sharper with increasing the annealing temperature, indicating the enhancement of crystallinity. As a result of annealing, the corresponding FWHM of the peaks decreases and the particle size increases as authenticated by Scherer (Fig. 3) and the Williamson–Hall (W-H) plot (Fig. 4). Ge QDs have a number of defects such as oxygen vacancies and lattice disorders. Through the annealing process these defects are removed and the lattice contracts. Also lattice relaxation due to dangling bonds should be considered. The dangling bonds on Ge surface interact with oxygen ions from the atmosphere and due to electrostatic attraction, and the lattice is slightly contracted. The diamond lattice parameters such as the values of d, which is the distance between adjacent planes in the Miller indices (hkl) (calculated from the Bragg equation), lattice constants and unit cell volumes as a function of annealing temperature are summarized in Table 1.

Table 1. The structure parameters of Ge QDs (extracted from XRD spectra). LP: lattice parameter.

Sample	hkl	2θ	d_{hkl} (nm)	LP (nm)	V (nm^3)
$A_{300}S_{10}G_5$	(111)	27.30	0.326		
	(220)	45.40	0.199	0.565	0.180
$A_{500}S_{10}G_5$	(111)	27.40	0.325		
	(220)	45.55	0.198	0.562	0.177
$A_{700}S_{10}G_5$	(111)	27.65	0.322		
	(220)	45.65	0.198	0.559	0.174

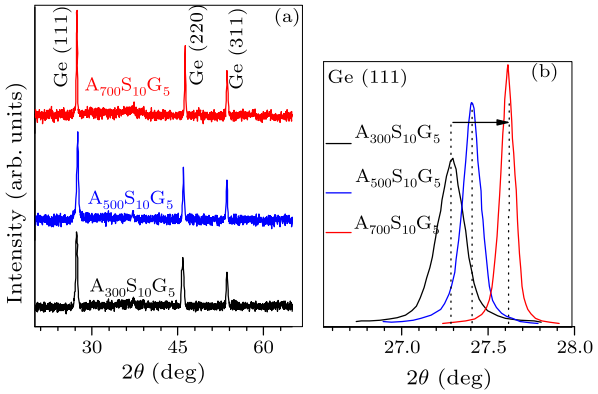

Fig. 2. (a) The XRD pattern of samples at different annealing temperatures. (b) The XRD pattern shows that the sample product is crystalline with a diamond FCC. High magnification spectra between $2\theta = 26.5°$ and 28°.

Figure 2(b) clearly displays the considerable shift in (111) peak position towards higher angle due to the increase of annealing temperature. This is interpreted in terms of change in interatomic distances and decreasing the lattice parameters. The deviation in the peak position can be explained into macroscopic strain. Several reasons are possible for this decrement such as elimination of defects and structural relaxation. XRD can be utilized to evaluate peak broad-

ening with crystallite size and lattice strain due to dislocation.[9] The particle size of the Ge QDs is determined by the x-ray line broadening method using the Scherrer equation

$$D = (\lambda k/\cos\theta\beta_{\rm D}), \tag{1}$$

where D is the particle size in nanometers, λ is the wavelength of the radiation (1.54056 Å for CuKa$_1$ radiation), k is a constant equal to 0.94, $\beta_{\rm D}$ is the peak width at half-maximum intensity, and θ is the peak position. The breadth of the Bragg peak is a combination of both instrument and sample dependent effects. To decouple these contributions, it is necessary to collect a diffraction pattern from the line broadening of a standard material such as silicon to determine the instrumental broadening. The instrument-corrected broadening $\beta_{\rm D}$ corresponding to the diffraction peak of Ge is estimated using the relation[10]

$$\beta_D^2 = [\beta^2_{\rm measured} - \beta^2_{\rm instrument}]. \tag{2}$$

Plots are drawn with $\lambda k/\beta_{\rm D}$ on the x-axis and $\cos\theta$ along the y-axis for the Ge QDs at different annealing temperatures such that the preferred orientation peaks of Ge with the diamond phase appear between $2\theta = 20^\circ$ and 75°. By fitting the data, the crystallite size D is extracted from the slope of the fit line, see Fig. 3.

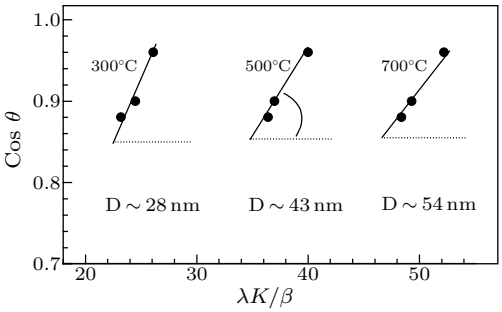

Fig. 3. Sherrer plot of samples at different annealing temperatures. Fit to the data, the crystalline size D is extracted from the slope of the fit.

Strain-induced broadening arising from crystal imperfections and distortion are related by $\varepsilon = \beta_{\rm s}/\tan\theta$. A remarkable property of the Scherrer equation is the dependence on the diffraction angle θ. The W-H method does not follow a $1/\cos\theta$ dependence as in the Scherrer equation, but varies with $\tan\theta$. This fundamental difference allows for a separation of reflection broadening when both small crystallite size and microstrain ε occur together. The different approaches presented in the following assume that the size and strain broadening are additive components of the total integral breadth of a Bragg peak.[11] The distinct θ dependences of both effects lay the basis for the separation of size and strain broadening in the analysis of Williamson and Hall. Addition of the Scherrer Eq. (1) and $\varepsilon = \beta_{\rm s}/\tan\theta$ in the following equations results in

$$\beta_{hkl} = \beta_{\rm s} + \beta_{\rm D}, \tag{3}$$

$$\beta_{hkl} = \left(\frac{\lambda k}{D\cos\theta}\right) + 4\varepsilon\tan\theta. \tag{4}$$

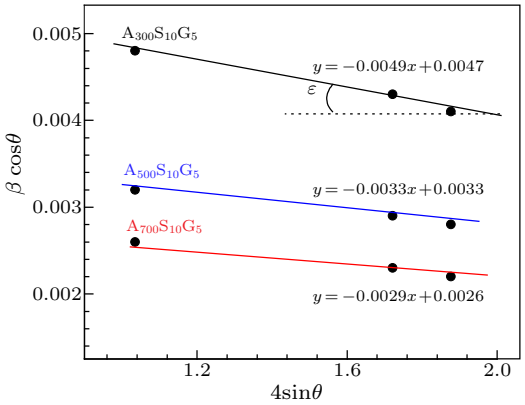

Fig. 4. The W-H plot of samples at different annealing temperatures assuming the uniform deformation model. Fit to the data, the strain and size are extracted from slope and y-intercept of the fit, respectively.

Rearranging Eq. (4) gives

$$\beta_{hkl}\cos\theta = \left(\frac{\lambda k}{D}\right) + 4\varepsilon\sin\theta, \tag{5}$$

which represents the uniform deformation model, where the strain is assumed to be uniform in all crystallographic directions. Thus considering the isotropic nature of the crystal, all the material properties are independent of the direction along which they are measured. The term $(\beta\cos\theta)$ is plotted with respect to $(4\sin\theta)$ for the preferred orientation peaks of Ge QDs with the face center cubic diamond phase. The results of the W-H analysis are shown in Fig. 4 and tabulated in Table 2. Accordingly, the slope and y-intersect of the fitted line represent strain and particle size, respectively. The plots show a negative strain. This strain may be due to the lattice shrinkage that is observed in the calculation of lattice parameter. Increasing the SiO_2 inter-diffusion in the Ge layer and dots via annealing is the reason for decreasing strain by annealing temperature in the SiO_2-Ge interface region.

Table 2. Geometric parameters of Ge QDs annealed at 300℃, 500℃ and 700℃.

Sample	Scherrer Size (nm)	W-H Size (nm)	W-H ε (10^{-3})	W-H Size (nm) Width	W-H Size (nm) Height	AFM rms (nm)	AFM Number density (10^{11} cm^{-2})
$A_{300}S_{10}G_5$	28±1	29±1	4.9±0.02	30±2	6±1	0.9±0.1	0.9±0.05
$A_{500}S_{10}G_5$	43±1	42±1	3.3±0.02	44±2	8±1	1.3±0.1	0.6±0.05
$A_{700}S_{10}G_5$	54±2	53±1	2.6±0.02	57±3	11±2	1.5±0.1	0.7±0.05

Figure 5 illustrates the FTIR absorption spectra of the samples with different annealing temperatures. The well-known symmetric stretching and asymmetric stretching absorption modes of the Si–O and Ge-O bond[12] are shown. The as-deposited sample has many kinds of point defects, including neutral oxygen vacancies and non-bridging oxygen hole centers, which act as radiative recombination centers or so-called luminescence centers. Post-annealing treatment improves the matrix stoichiometry. The type and density of the point defects are expected to change with the post-annealing treatment. Increasing the annealing temperature to 500℃ leads to the formation of Ge suboxides by the reaction of extra silicon atoms existing in the off-stoichiometric SiO_x ($x < 2$) with the Ge oxides cases to increase the Ge–O bond intensity. It appears that the intensity of this peak decreases at the annealing temperature 700℃, implying that Ge–O bonds are diminished due to the decrease of GeO_x, which is exhausted at 700℃.

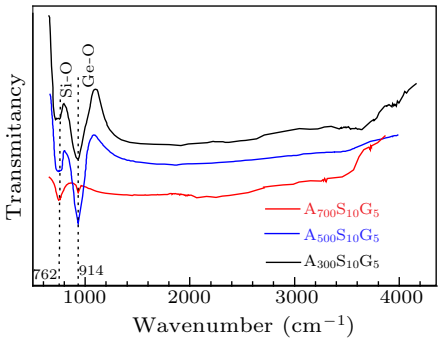

Fig. 5. FTIR spectra showing the effect of annealing temperature on the Ge/SiO_2/Si heterolayers containing QDs on the surface. Peaks related to Si–O and Ge–O linkage are shown with the dotted line and the corresponding wave number in units of cm^{-1}.

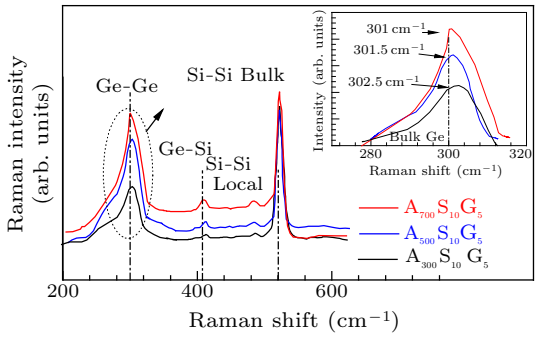

Fig. 6. Raman spectra of the samples at different annealing temperatures. Inset: the high magnification of Ge–Ge phonon vibration shift.

Figure 6 indicates the Raman spectra of the samples annealed at various temperatures. Each spectrum displays four asymmetrical Raman peaks around 300, 415, 490 and 520 cm^{-1}, typically corresponding to the scattering from optical phonons involving Ge–Ge, Ge-Si, localized Si–Si motion in the neighborhood of one or more Ge atoms in the SiO_2 matrix, and Si–Si vibration modes, respectively. Increasing the Ge–Ge peak intensity is attributed to the improvement of Ge QDs crystallinity and is in agreement with the XRD results.

The Ge–Ge peak is right-shifted with respect to the peak of bulk Ge (300 cm^{-1}). At 300, 500, and 700 annealing temperatures, these peaks appear at 302.5, 301.5 and 301 cm^{-1}, respectively (the inset of Fig. 6). The observed peak shift is due to the competitive effects of quantum confinement of localized phonons in the disordered nanostructure and the strain relaxation.[13] The strong confinement effect in the vertical direction of the QDs due to its much smaller dimension (height ∼6–12 nm) compared with the exciton Bohr radius of Ge (24 nm) is attributed to the probable shift towards lower frequency. Effectively, strain played a predominant role in shifting the peak towards higher frequency which has been addressed.[14] During and after the growth process, GeSi intermixing takes place, enhanced by high annealing temperatures. The chemical reactions between the Si-Ge alloy and the reduction of mismatch energy at the phase boundary are two thermodynamic driving forces, which propose the temperature-enhanced intermixing and alternate path to the strain relaxation, which is in good agreement with the W-H plot. The signature of the intermixing and its enhancement by temperature is evidenced as the Ge–Si peak in the Raman spectra (Fig. 6).

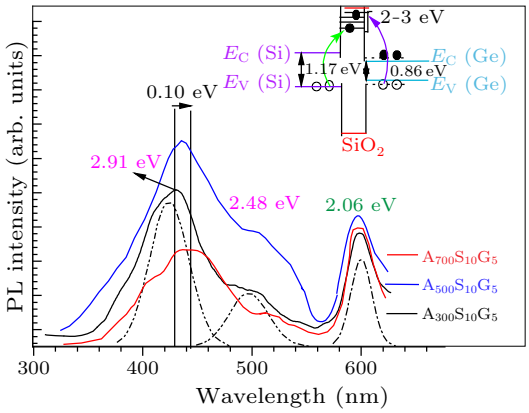

Fig. 7. PL spectra of the samples at different annealing temperatures. Inset: the band diagram and emission mechanism.

Figure 7 shows the PL spectra from the samples annealed at different temperatures. There are two main peaks which are centered at 2.91 and 2.06 eV accompanied by a weak shoulder at 2.48 eV. The PL red shift of ∼0.10 eV, caused by increasing the size of QDs due to the heat treatment, confirms quantum confinement. Furthermore, the silicon inter-diffusion is the dominant coarsening mechanism for the higher annealing temperature, and it decreases the compressive stress, shifting the peak to a lower energy value. With the increase of temperature, the intensity of peak increases and reaches its maximum at 500℃, then decreases. In our experimental range, the intensity of green PL at 2.06 eV keeps constant with the increase of temperature. From the results of FTIR spectra mentioned earlier, it is confirmed that the interface region of Ge dots with surrounding SiO_2 matrix for

$A_{300}S_{10}G_5$ sample occupied by Ge oxides. The Si–O bond is stronger and more stable than the Ge–O bond. Therefore, during annealing the extra silicon atoms existing in the off-stoichiometric SiO_x ($x < 2$) will react with the Ge oxides to produce Ge suboxides or elemental Ge. Thus the content of GeO increases in the films annealed at the starting temperature below 500℃, results in an increase of the number of luminescence centers to reach the maximum. With a higher annealing temperature, GeO_x ($x > 1$) are almost exhausted as clearly appeared at FTIR spectra, and the content of GeO decreases dramatically, resulting in the decrease of the number of photo-carriers and decrease of the PL intensity.

Possible origins of the observed PL are defect-related luminescent centers in the matrix and interface. Since PL bands under our experimental conditions show different behaviors with the annealing temperature additions, the two PL bands should have different origins. Different types of defects in silicon dioxide, e.g., non-bridging oxygen hole centers, can emit visible orange-green PL bands centered in the energy range of 2.3–2.6 eV.[15] In our work, Ge/SiO_2 films were uniformly deposited on silicon substrates and nc-Ge formed during annealing through demixing and nucleation of small crystals. During nanocrystal growth, oxygen deficit defects will form in silicon oxide matrix. Therefore, defects related to the oxygen deficits may be one origin of our observed PL. On the other hand, highly disturbed bonds in the inhomogeneous strain field of Ge nanocrystal surfaces may also be responsible for the appearance of PL after annealing. The crystallization process is associated with cleaning and reconstruction, which causes out-diffusion of the last traces of oxygen during the growth of nc-Ge. GeO_2 defects containing two non-bonding electrons have been reported by Ginzburg *et al.*,[16] and Gallagher and Osterberg[17] in Ge-doped silica glass fibers. Such defects create a ground-state singlet level (S0), an excited singlet level (S1), and a triplet level (T1). The radiative recombination requires the energy ∼2.91 eV. However, to confine electrons with energies ∼2 eV above the conduction band edge the potential barrier at the Ge-dot is not sufficient for such recombination. This fact suggests that the radiative recombination does not involve electrons from the conduction band of the Ge or Si, rather it involves localized electrons transition from T1→S0 in radiative defect states at the Ge-dot/SiO_2 interfaces. The origin of 2.48 and 2.06 eV peaks can be attributed to recombination of electrons in the S1 level and hole in the ground state level at Ge and Si valence bands, respectively, as shown in the inset of Fig. 7.

In summary, Ge QDs embedded with $Ge/SiO_2/Si$ hetero-structure have been prepared using the rf magnetron sputtering method. The effects of post-annealing temperature on surface morphology and optical properties are determined. The broadening of XRD peaks with the decrease of annealing temperature from 700℃ to 300℃ is ascribed to the decrease of crystallite size and lattice strain enhancement. The Scherrer and W-H plot confirms the broadening effects. Dot density, size and occupancy are discerned to be strongly dependent on annealing temperature, where Ge QDs recrystallization is promoted by Si–O bond formation. Both the room temperature PL and Raman spectra exhibit intense and broad peaks accompanied by a shift depending on annealing temperature. Quantum confinement of carriers in the Ge QDs and the role of strain are mainly responsible for the shift. It is reaffirmed that the present low temperature growth mode of Ge QDs is prospective for the development of nanoscale materials beneficial for devices. This in-depth measurement followed by analysis is believed to strengthen the basic insight involving the physics of growth of sputtering-assisted heterostructure layers and their generic properties at nano-scale. This knowledge is useful for fabrication of devices such as biosensors and full-color display, integrated optoelectronics technology, where a precise and versatile control of the surface and optical properties is pre-requisite.

References

[1] Lee S, Huang S, Conibeer G and Green M 2014 *Appl. Surf. Sci.* **290** 167
[2] Samavati A, Othaman Z, Ghoshal S K and Zare S 2013 *Chin. Opt. Lett.* **11** 112502
[3] Samavati A, Mustafa M K, Othaman Z and Ghoshal S K 2015 *J. Nanomater.* **2015** 681242
[4] Bhatt V and Chandra S 2007 *J. Micromech. Microeng.* **17** 1066
[5] Samavati A, Othaman Z, Ghoshal S K and Dousti M R 2014 *J. Lumin.* **154** 51
[6] Samavati A, Othaman Z, Ghoshal S K and Amjad R J 2013 *Chin. Phys.* B **22** 098102
[7] Leifeld O, Beyer A, Grutzmacher D and Kern K 2002 *Phys. Rev.* B **66** 125312
[8] Kashtiban R J, Pinto S R C, Bangert U, Rolo A G, Chahboun A, Gomes M J M and Harvey A J 2010 *J. Phys.: Conf. Ser.* **209** 012060
[9] Yogamalar R, Srinivasan R, Vinu A, Ariga K and Bose A C 2009 *Solid State Commun.* **149** 1919
[10] Rogers K D and Daniels P 2002 *Biomaterials* **23** 2577
[11] Samavati A, Othaman Z, Dabagh S and Ghoshal S K 2014 *J. Nanosci. Nanotechnol.* **14** 5266
[12] Khan A F, Mehmood M, Ali T and Fayaz H 2013 *Thin Solid Films* **536** 220
[13] Sugai S, Sotokawa H, Kyokane D and Onodera A 1996 *Physica* B **219** 293
[14] Macedo J G, Aguilar G V, Gomez R W, Perez-Mazariego J L and Marquina V 2008 *J. Nanosci. Nanotechnol.* **8** 1
[15] Stutzman M 1995 *Phys. Status Solidi* B **192** 273
[16] Ginzburg L P, Gordeev A A, Gorchakov A P and Jilinsky A P 1995 *J. Non-Cryst. Solids* **183** 234
[17] Gallagher M and Osterberg U 1993 *J. Appl. Phys.* **74** 2771